Vibrational spectroscopy of functional group chemistry and arsenate coordination in ettringite

Satish C. B. Myneni,[1,*] Samuel J. Traina,[1] Glenn A. Waychunas,[2] and Terry J. Logan[1]

[1]School of Natural Resources, Kottman Hall, The Ohio State University, Columbus, Ohio 43210, USA
[2]Earth Sciences Division, Lawrence Berkeley National Laboratory, Berkeley, California 94720, USA

Abstract—The functional group chemistry and coordination of AsO_4^{3-}-sorption complexes in ettringite $[Ca_6Al_2(SO_4)_3(OH)_{12} \cdot 26H_2O]$ were evaluated as a function of sorption type (adsorption, coprecipitation) and pH using Raman and Fourier Transform infrared (FTIR) spectroscopies. The reactive functional groups of ettringite, $\equiv$Al-OH, $\equiv$Ca-OH$_2$, and $\equiv$Ca$_2$-OH, exhibit broad overlapping OH bands in the range 3600–3200 cm^{-1}, prohibiting separation of component vibrational bands. The SO_4^{2-} polyhedra of the channels are present in three crystallographically different sites and exhibit weakly split S-O asymmetric stretch at 1136 cm^{-1} (with several components) and symmetric stretch at 1016, 1008, and 989 cm^{-1}. During AsO_4^{3-} adsorption, the vibrational spectra of SO_4^{2-} were least affected, and the OH stretching intensities around 3600 cm^{-1} decreased with an increase in AsO_4^{3-} sorption. In contrast, the S-O symmetric stretch at 1016 and 1008 cm^{-1} were almost completely removed, and the OH vibrations were relatively unaffected during AsO_4^{3-}-coprecipitation. The As-O asymmetric stretch of sorbed AsO_4^{3-} are split and occur as overlapping peaks around 870 cm^{-1}. The As-O$_{complexed}$ stretching vibrations are at ~800 cm^{-1}. The low pH samples (pH = 10.3–11.0) exhibit distinct As-OH stretching vibrations at 748 cm^{-1}, indicating that some of the sorbed AsO_4^{3-} ions are protonated. These spectral features demonstrate that AsO_4^{3-} directly interacts with ettringite surface sites during adsorption and substitute inside the channels during coprecipitation (preferentially for two of the three sites). The energy position of the As-O symmetric stretch vibrations suggest that the AsO_4^{3-} polyhedra interacts predominantly with $\equiv$Ca-OH$_2$ and $\equiv$Ca$_2$-OH sites rather than with $\equiv$Al-OH sites. Sorption of more than one type of As species was evident in low pH (<11.0) samples. *Copyright © 1998 Elsevier Science Ltd*

1. INTRODUCTION

Oxoanions, arsenate (AsO_4^{3-}), chromate (CrO_4^{2-}), and selenate (SeO_4^{2-}) are common contaminants in natural aquatic environments, and their interactions with mineral surfaces determine their solubility, speciation, and transport properties. Several minerals with a potential to react with oxoanions in acid to neutral solution have been identified, and research is in progress to gain knowledge on molecular mechanisms responsible for oxoanion sorption and toxicity in these systems (Hingston et al., 1967; Harrison and Berkheiser, 1982; Hayes et al., 1987; Mulcahy et al., 1990; Reeder et al., 1994; Persson et al., 1996; Hug, 1997; Waychunas et al., 1993). However, alkaline solutions containing toxic oxoanions pose a serious environmental problem since anion sorption by common mineral substrates is greatly diminished under these conditions. Past research has shown that ettringite $[Ca_6Al_2(SO_4)_3(OH)_{12} \cdot 26H_2O]$, a Ca-Al-sulfate, is stable in alkaline materials and sorbs oxoanions into its structure. In geologic materials, ettringite is often found in low temperature hydrothermal mineral deposits and alkaline evaporites and has been proposed to be a primary mineral in incorporating U and other element oxoanions from contacting solutions (Linklater et al., 1996). In addition, precipitation of ettringite with the incorporation of SO_4^{2-}, SO_3^{2-}, $B(OH)_4^-$, CO_3^{2-}, and other oxoanions from the leachate of alkaline in-

dustrial byproducts (flyash), cements, and cement-based waste matrices has serious repercussions to the strength of the cements and their hydraulic properties (porosity, permeability) and the quality of surface and subsurface water in their vicinity (Mattigod et al., 1990; Fowler et al., 1993; Mehta and Monteiro, 1993). Because of its environmental significance, several researchers have examined the role of ettringite in toxic metal sorption and its stability in natural Eh-pH conditions (Pöllmann et al., 1989; Kumarathasan et al., 1990; Myneni et al., 1997; Myneni et al., 1998a). Our research emphasis has been primarily on the surface chemistry of ettringite and the AsO_4^{3-} molecular interactions in ettringite (Myneni, 1995). The stability of AsO_4^{3-} complexes on ettringite surfaces are determined by the type of sorption complexes, their solvation, protonation, and location in ettringite structure. Since As is a common pollutant in alkaline flyash, and these materials have been proposed for use in solidification and attenuation of complex waste streams, information on AsO_4^{3-} coordination in ettringite is of geochemical significance.

The ettringite crystal structure consists of columns of $\{Ca_6[Al(OH)_6]_2 \cdot 24H_2O\}^{6+}$ with the intercolumn space (channels) occupied by anions such as SO_4^{2-} and H_2O molecules (Fig. 1). The column H_2O molecules form H-bonds with channel ions and hold the columns together through electrostatic interactions. Thus, oxoanion sorption (adsorption and/or coprecipitation) in ettringite results in channel substitution (by replacing SO_4^{2-}, H_2O) and/or formation of complexes with surface functional groups (by replacing OH, H_2O). Macroscale (sorption, mass balance, thermodynamics; Myneni et al., 1997)

---

*Author to whom correspondence should be addressed (smyneni@lbl.gov).
Present address: Mail Stop 90/1116, Earth Sciences Division, Lawrence Berkeley National Laboratory, Berkeley, California 94720, USA.
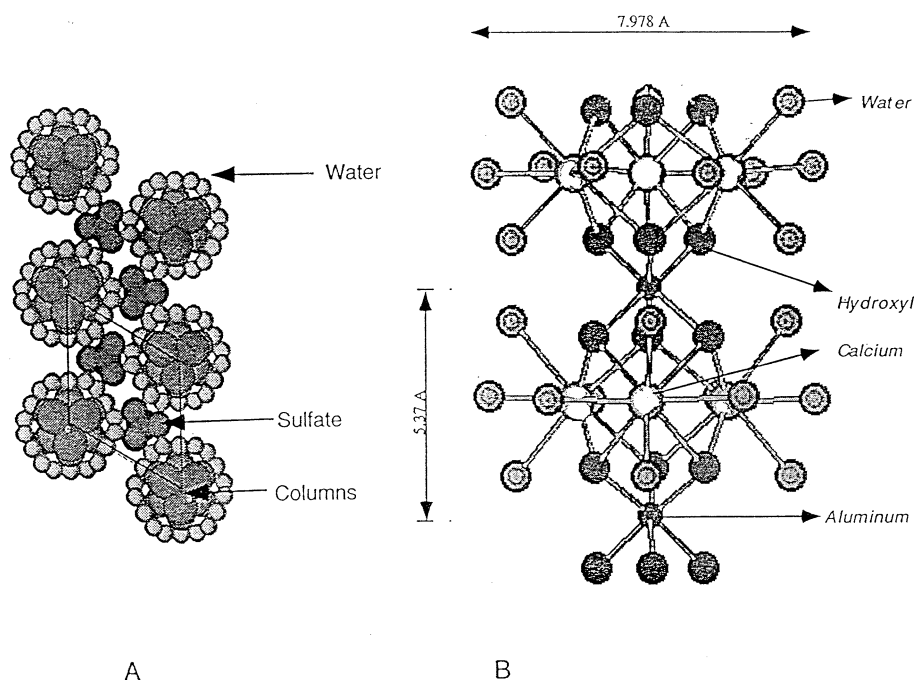
Fig. 1. Ettringite crystal structure. (A) (001) plane, showing columns and channels, with the unit cell dimensions marked. (B) structure of a single column with Al (small dark) and Ca (hollow) atoms coordinated by OH and H_2O molecules. Calcium coordinated H_2O and OH^- are shown as light and large dark spheres (for structural parameters, see Moore and Taylor, 1970). The dimensions are shown with a scale bar on either side of crystal structure (for b), and this scale do not correspond to Fig. 1a.

and spectroscopic studies (Extended X-ray Absorption Fine Structure (EXAFS) & vibrational; Myneni, 1995) have been conducted to evaluate AsO_4^{3-} interactions with ettringite in alkaline materials. While the EXAFS studies have offered direct evidence on the AsO_4^{3-} coordination in ettringite, the chemistry of surface OH/H_2O functional groups and their interactions with AsO_4^{3-} polyhedra could not be obtained from them. Vibrational spectroscopy, specifically the Fourier Transform infrared spectroscopy (FTIR), can be used to obtain symmetry and structural information of reactive groups, such as OH and H_2O present in ettringite. By combining FTIR with Raman spectroscopy, complete vibrational spectral information of AsO_4^{3-}-ettringite complexes can be obtained. In this paper, we present the vibrational spectroscopy evaluation of ettringite functional group chemistry and the coordination environment of AsO_4^{3-} in ettringite as influenced by the mode of sorption (adsorption vs. coprecipitation).

1.1. Vibrational Spectroscopy of Arsenate

Arsenate is a tetrahedral molecule and exhibits four fundamental vibrations, an A_1 (symmetric stretch, ν_1), an E (symmetric bending, ν_2), and two F vibrations (asymmetric stretching & bending, ν_3 & ν_4, respectively; Nakamoto, 1986). The vibrations E and F are doubly and triply degenerate modes, respectively. Protonation, metal complexation, and/or adsorption on ettringite surfaces should cause sufficient changes in AsO_4^{3-} symmetry (from tetrahedral to other lower symmetries, such as C_{3v}, C_{2v}, C_1) to cause the degenerate vibrations of AsO_4^{3-} to split and the As-OX (X = H^+, H_2O, metal) stretch-

ing to shift to different wavenumbers. It should be noted that the detection of spectral splitting depends on the symmetry deviation and how well the individual components can be resolved. For these reasons some AsO_4^{3-} complexes in lower symmetry may not exhibit any splits in the degenerate vibrations. A complete discussion of symmetry changes and associated vibrational spectra of AsO_4^{3-} is discussed elsewhere (Myneni et al., 1998b). Altogether, the group frequencies of AsO_4^{3-} can be used to interpret the symmetry and the nature of surface complexes when AsO_4^{3-} is not protonated. However, metal complexation of protonated AsO_4^{3-} does not significantly change the AsO_4^{3-} group frequencies, and these are of little use in predicting the symmetry of AsO_4^{3-} sorption complexes in minerals. Clearly, it is essential to establish the nature of AsO_4^{3-} sorption complex (protonated vs. unprotonated) before its coordination environment is evaluated. Our previous studies have also shown that the AsO_4^{3-}-solvated H_2O molecules exhibit OH stretching and bending vibrations at energies different from that of bulk H_2O. Such spectral changes for OH vibrations (especially the stretching vibrations) are useful in exploring the AsO_4^{3-}-coordinated H_2O or OH on mineral surfaces.

The only previous IR study on AsO_4^{3-}-substituted (coprecipitated) ettringite was conducted by Kumarathasan et al. (1990), who reported a single peak for As-O ν_3 vibrations (873 cm^{-1}). Due to the preservation of degeneracy for the As-O ν_3 vibrations, it can be argued that AsO_4^{3-} may retain its tetrahedral symmetry and probably forms outer-sphere, ion pairs in ettringite. However, other IR studies on crystalline calcium arsenates (Moenke, 1962; Ross, 1974; Myneni et al., 1998b)

have shown that As-O ν_3 vibrations are split, indicating a lower symmetry than tetrahedral for AsO_4^{3-} in these chemically analogous materials. These studies do assist in band identification, yet they are of little utility in evaluating the coordination of AsO_4^{3-} complexes in ettringite. AsO_4^{3-} in C_1 and C_{2v} symmetries produce the same number of bands and the amount of splitting varies with the type of complexing metal and the number of metal atoms bound to AsO_4^{3-} (Nakamoto, 1986; Myneni et al., 1998b). Thus sorption environments corresponding to these different symmetries can not always be ascertained from the vibrational spectra. In addition, the sorption of protonated and unprotonated AsO_4^{3-} exhibit completely different types of spectral features even when they form the same type of complexes. In the present study, we have correlated the vibrational spectra of ettringite to the X-ray crystal structure analysis conducted by Moore and Taylor (1970) in an effort to better understand the coordination chemistry of the reactive functional groups in ettringite. Additionally, we have used this data, vibrational spectra of AsO_4^{3-} in ettringite, and the vibrational spectra of calcium arsenate minerals of known crystal structure, to ascertain the local coordination chemistry and site symmetries of AsO_4^{3-} in ettringite.

While the notations A, E, and F; ν_1, ν_2, ν_3, and ν_4; and As-OX (X = metal, H$^+$, H$_2$O), and As-O$_{uncomplexed}$ are commonly used to refer to the different vibrational modes of AsO_4^{3-}, we adopted the latter notation since this has information on the actual vibrating atom-pair. As discussed later, several of the As-O vibrations strongly overlap each other and their component vibrations can not be separated without ambiguity. In such occasions we used nonspecific terminology, such as As-OX or As-O$_{uncomplexed}$ vibrations without referring to the symmetric or asymmetric type of stretching. The vibrational spectra of SO_4^{2-} was also discussed in the same fashion.

2. EXPERIMENTAL SECTION

2.1. Ettringite Synthesis and Arsenate Sorption

Ettringite was synthesized under N_2 (g) by mixing $Al_2(SO_4)_3$ and CaO in 10% sucrose solution. While AsO_4^{3-} adsorption experiments were conducted by reacting synthetic ettringite with CO_2-free aqueous solutions of $Na_2(HAsO_4) \cdot 7H_2O$, the coprecipitation studies were directed at precipitating ettringite from arsenate and sulfate containing solutions. Adsorption and coprecipitation experiments were conducted over a range of AsO_4^{3-} concentrations ($<$1 μM–15 mM) and pH values (10.0–12.5). In pH controlled experiments, 0.1 M NaOH and HCl were used to attain required suspension pH. The details of the synthesis procedures and the precipitate chemical analysis are described by Myneni et al. (1997) and Myneni et al., 1998a. A summary of these studies are provided in Table 4 and briefly discussed later.

2.2. Data Collection and Analysis

Diffuse reflectance FTIR spectra of powdered samples were collected on a Mattson Polaris FTIR. The samples were diluted to a concentration of 2% with IR-grade KBr. Two hundred co-added scans were collected at 1 cm^{-1} resolution in the mid-IR region (4000–400 cm^{-1}) for pure KBr and for each KBr-mixed sample. Vibrational spectra of each sample were obtained by subtraction of the background spectra (pure KBr) from the sample + KBr spectra. The structure and coordination of aqueous AsO_4^{3-} and SO_4^{2-} were examined using the attenuated total reflection Fourier Transform infrared spectroscopy (ATR-FTIR; ZnSe crystal). The ZnSe ATR-element used in this study was a prism with a size of $8 \times 8 \times 33$ mm and has nine reflections. The incident IR beam has a 45° angle with the surface of the ZnSe ATR element. The ZnSe crystal was washed with deionized water at the end

of each sample scan. To minimize oxoanion reactions with the ZnSe crystal, the spectra were collected immediately after the solutions were transferred into the ATR cell. However, the spectra were invariant from $<$0.017 h to 1 h. Background subtractions were made to remove the bulk water spectra. The aqueous solutions of these oxoanions were prepared by dissolving reagent grade $Na_2HAsO_4 \cdot 7H_2O$ and Na_2SO_4 in deionized water. Raman spectroscopic studies were conducted using a Ti: sapphire laser (Coherent) operating at 784 nm and a single stage spectrograph (Instruments SA, HR 640) with a 300 mm^{-1} grating coupled to a CCD. The scans ranged from 2000 to 200 cm^{-1}, with a step-size of 1.5 cm^{-1}. The superimposed spectra were deconvoluted for the number of bands and their energy positions using the spectral second derivatives. Using this information, the overlapped peaks were fit with Cauchy-Laurenzian profiles, or a mixture of Cauchy-Laurenzian and Gaussian profiles. This is because the previous studies have indicated that the IR peaks exhibit predominantly Lorentzian shape with little or no Gaussian character (Maddams, 1980). The dilute aqueous arsenate and As-ettringite spectra were smoothed using Savitzky-Golay function (10–15 points, second-order polynomial). The details of instrument setting and spectral analysis were the same as those described by Myneni et al. (1998b).

2.3. Bond Valence Estimates

Bond valence calculations for O atoms of the surface functional groups, $\equiv$Ca-OH$_2$, $\equiv$Ca$_2$-OH, $\equiv$AlCa$_2$-OH, and $\equiv$Al-OH (the symbol $\equiv$ denotes crystal surface), were conducted as described in Brown and Altermatt (1985). Proton contribution at the O atoms were not considered during these calculations, since the bond lengths of OH groups present on the mineral surfaces are not known. Also, it may be improper to assign bulk OH bond lengths to the surfaces, since the surface OH units are different from the bulk in their H-bonding to the adsorbed H_2O molecules. This has been clearly shown in the diffuse reflectance infrared spectroscopy studies of iron oxide phases (Parfitt et al., 1976; Tejedor-Tejedor and Anderson, 1986).
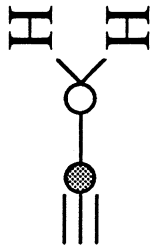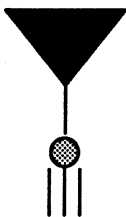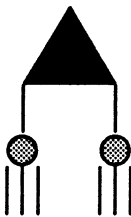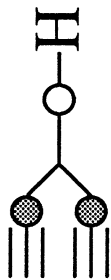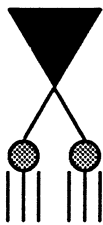
3. RESULTS AND DISCUSSION

Arsenate sorption in ettringite may result in the formation of surface complexes (corner-, edge-sharing) and/or isomorphic substitution for SO_4^{2-} in ettringite channels. Based on Pauling's Second Rule and the valence units (v.u.) of cation contribution at the linking O of the surface functional groups (Brown and A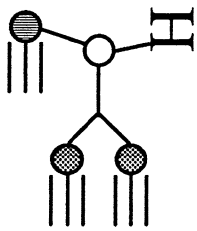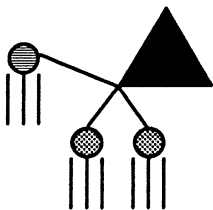ltermatt, 1985; Bargar et al., 1997), it is evident that these sites will exhibit a preference for AsO_4^{3-} sorption leading to the formation of edge- or corner-sharing complexes (Myneni et al., 1997). Ettringite has $\equiv$Ca-OH$_2$, $\equiv$Ca$_2$-OH, $\equiv$AlCa$_2$-OH, and $\equiv$Al-OH sites on the (001) faces and predominantly $\equiv$Ca-OH$_2$ on all other exterior faces and inside the channels (Fig. 1, Table 1). During sorption, AsO_4^{3-} directly interacts with these $-$OH or $-$OH$_2$ surface sites through ligand exchange and forms $\equiv$Ca-O-AsO$_3$, $\equiv$Ca$_2$-O-AsO$_3$, $\equiv$Al-O-AsO$_3$ complexes (in the case of monodentate corner-sharing complexes (Table 1). Ligand exchange is unwarranted and complexes such as

$$\begin{array}{c} H \\ | \\ \equiv Ca\text{-}O\text{-}AsO_3 \end{array}$$
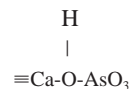
are not possible, because the As-OH bond is already saturated (As-O: 1.25 v.u., O-H: ~0.78 v.u.) and can only form H-bonds. Similar behavior is seen in several crystalline solids containing protonated arsenate (Myneni et al., 1998b). The sum of v.u. contribution from the cations at the linking O atoms of these complexes are 1.43, 1.85, and 1.76 v.u., respectively (Table 1). Consequently, to satisfy electroneutrality the $\equiv$Ca-O-AsO$_3$ requires relatively high cationic contribution (0.57 v.u.) to have a stable complex. Although this can be provided by H-bonding

Table 1. Types of possible AsO_4^{3-} complexes in ettringite.

Surface functional groups in ettringite	AsO_4^{3-} complexation with ettringite functional groups	Sum of Bond Valence contribution at the 'O' atom[*], After AsO_4^{3-} complexation
		1.43 (at each of the linking O atom)
		1.85
		1.76
		2.37

$\bigcirc$:oxygen, : surface Ca, : surface Al, ▲: AsO_4^{3-}

* Bond valence is estimated as described by Brown and Altermatt (1985).

with at least 3 H_2O molecules, such interactions are restricted inside the channels due to stearic hindrance. Yet, these types of complexes can be formed on the surface sites where stearic limitations are minimal. Similarly, the other two surface complexes ($\equiv Ca_2$-O-AsO_3, $\equiv$Al-O-AsO_3) are also favorable, by accepting H-bond contribution from surrounding H_2O molecules. Edge-sharing complexes at these sites have to satisfy the same conditions discussed above for corner-sharing complexes and additionally the length of an edge in As polyhedra must be similar to those of Ca and Al for these complexes to form. Finally the geometry of AsO_4^{3-} polyhedra in edge-sharing complexes does not allow extensive H-bonding with H_2O molecules. This limits the formation of edge-sharing complexes with $\equiv$Ca-OH_2 sites in the channels. However, the surface $\equiv Ca_2$-OH and $\equiv$Al-OH sites can form edge-sharing complexes with AsO_4^{3-}. The $\equiv AlCa_2$-OH site can not form complexes with AsO_4^{3-}, because the O atom is already saturated, and if complexation with AsO_4^{3-} occurred, the bond valence at the O would be >2.35 v.u. (Table 1).

These AsO_4^{3-} sorption reactions result in displacement of OH or H_2O from surface ($\equiv$Ca-OH_2, $\equiv Ca_2$-OH, $\equiv$Al-OH) or channel ($\equiv$Ca-OH_2) sites and changes in H_2O coordination with changes in H-bonding from SO_4^{2-} to AsO_4^{3-} (Myneni, 1995). Such changes alter the vibrational spectra of H_2O, SO_4^{2-}, $Ca(OH)_4(H_2O)_2^{2-}$, and $Al(OH)_6^{3-}$ units within ettringite. Since the Ca and Al polyhedra are already highly distorted in ettringite (variation in Ca-O, Al-O bond lengths are 2.35–2.75 Å, 1.82–2.00 Å, respectively, Moore and Taylor, 1970), AsO_4^{3-} complexation to their polyhedra may not cause additional changes in Ca-O and Al-O bond lengths and hence their vibrational bands. Also the overlap of OH bending vibrations with S-O and As-O v_2, and v_4 prevents accurate separation of their individual components. Hence this study focused on the O-H, S-O, and As-O stretching vibrations only. The results are presented under two sections: (1) ligand coordination and functional group chemistry in ettringite and (2) AsO_4^{3-} interactions in ettringite.

3.1. Ligand Coordination and Functional Group Chemistry in Ettringite

A vibrational spectrum of ettringite exhibits broad OH stretching peaks around 3550 and 3300 cm^{-1}, OH bending at 1640 cm^{-1}, CO_3^{2-} stretching at 1450 cm^{-1}, and SO_4^{2-} asymmetric and symmetric stretching around 1100 and 990 cm^{-1}, respectively (Table 2, Fig. 2). Below 800 cm^{-1}, several broad, overlapping bands appear which are due to S-O, C-O, and Al/Ca-OH bending vibrations. The functional group chemistry of different sites in ettringite is evaluated from their vibrational spectra and is discussed below.

3.1.1. OH and H_2O related vibrations

Liquid water exhibits three bands due to OH stretching and bending at 3615 (antisymmetric stretching), 3450 (symmetric stretching), and 1640 cm^{-1} (bending) in mid-IR region (Nakamoto, 1986). While the structural and surface OH in gibbsite and portlandite exhibit peaks at 3618, 3526, 3468, and 3398 cm^{-1} and 3642 and a broad band around 3300 cm^{-1}, respectively, the H_2O groups in gypsum shows strong IR absorption bands at 3550 and 3403 cm^{-1} (Fig. 3). When compared to these

Table 2. Vibrational spectra of ettringite and band assignments.

Band Position (± 10 cm⁻¹)		Band Assignment and Comments
Diffuse Reflectance FTIR	Raman	
3560		OH stretching of $\equiv$Al-OH, $\equiv Ca_2$-OH, $\equiv$Ca-OH_2
3400-3235		OH stretching of $\equiv$Ca-OH_2
1647		OH bending of $\equiv$Ca-OH_2, channel H_2O
1489-1430		CO_3^{2-} v_3 as. stretching
1138	1170-1129	SO_4^{2-} v_3 as. stretching
	1078	SO_4^{2-} as. stretching, CO_3^{2-} sym. stretching
989	990	SO_4^{2-} v_1 sym. stretching
872 (broad)	871-837	Al-OH bending vibrations, CO_3^{2-} v_2 sym. bending
	750-714	CO_3^{2-} v_4 as. bending
639-610	668-607	v_4 S-O, Ca-OH bending vibrations
547	555-542	Al-OH bending vibrations
	490-480	v_2 S-O
	450-430	v_2 S-O and/or S-OH bending vibrations
	373	Ca-O
346, 317*	344, 310	Ca-O
	289	Not assigned

* This data is collected in transmission mode.

structurally simple metal-hydroxides and sulfates, ettringite has several types of OH and these are: OH exposed at the surfaces ($\equiv$Al-OH, $\equiv Ca_2$-OH, $\equiv$Ca-OH_2), structural OH ($\equiv AlCa_2$-OH; $\equiv$Ca-OH_2, form H-bonds with channel SO_4^{2-}), and free OH^- and H_2O in the channels. These varieties of OH bonding environments produce broad IR absorption bands around 3550, 3300, and 1640 cm^{-1}, which are not conclusively resolved into individual vibrations (Fig. 3). From the second derivative and curve fitting of ettringite vibrational spectra, the observed peaks related to OH stretching vibrations are tentatively identified as: free OH (very weak peaks $\sim$ 3744 cm^{-1}, present only in high pH samples); Al-OH, Ca-OH (3650–3600 cm^{-1}); and Ca-OH_2
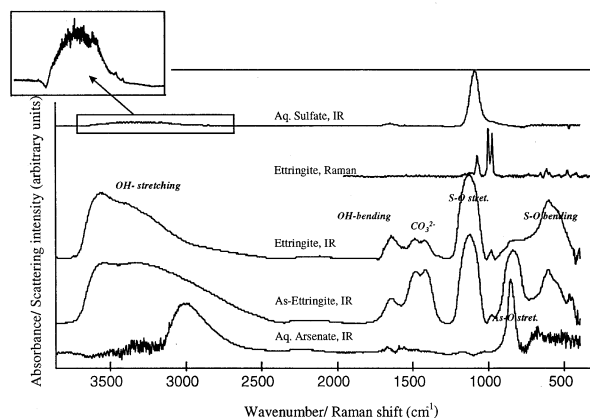
Fig. 2. Vibrational spectra of ettringite and related materials. The representative peaks in the spectra are: OH stretching, 3500–3000 cm^{-1}; OH bending (of H_2O) 1650 cm^{-1}; CO_3^{2-} v_3 vibrations, 1300–1500 cm^{-1}; SO_4^{2-}, 900–1250 cm^{-1}; AsO_4^{3-}, 1000–700 cm^{-1}; and other bend vibrations below 600 cm^{-1} (Table 2). Notice the correspondence of OH stretch of aqua ions and their corresponding features in their respective ettringite spectra.

Fig. 3. OH stretching vibrations of ettringite and related (for OH/H_2O coordination) minerals.

(3562, 3356 cm^{-1}). These band assignments were made after comparing with the vibrational spectra and X-ray crystal structure refinement data of gibbsite, gypsum, and portlandite (Siedl and Knop, 1969; Farmer, 1974; Pöllmann et al., 1989) and the vibrational spectra of solvated Ca^{2+} in the clay interlayers (Bishop et al., 1994). Since the Al-O and Ca-O bond lengths in these models and ettringite are similar, the relative strengths of Al-OH and Ca-OH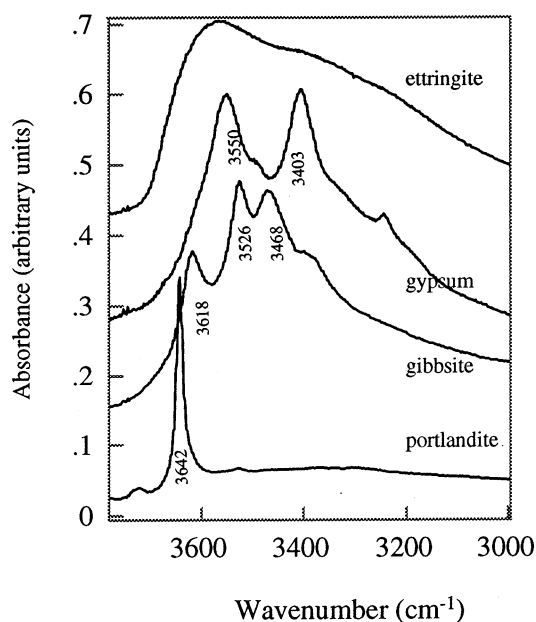/OH$_2$ are also expected to be similar and consequently their OH and H_2O vibrations (Fadini and Schnepel, 1989). However, H-bonding of ettringite functional groups with channel H_2O, OH, and/or SO_4^{2-} can modify OH and H_2O vibrations and produce small shifts from those of the structural models discussed earlier. Peaks related to OH bending vibrations are also observed at 1645, 916 and 541, 643 and 317 cm^{-1} corresponding to OH in H_2O, Al-OH, and Ca-OH, respectively (Fig. 2, Table 2).

The vibrations of H_2O and OH coordinated to Ca may not be significantly different, since the average Ca-O bond distances of Ca-OH (2.45 ± 0.05 Å) are smaller than those of Ca-OH$_2$ (2.55 ± 0.05 Å; Moore and Taylor, 1970). The OH bond lengths of Ca-OH$_2$ are expected to be longer due to extensive H-bonding between H_2O and channel SO_4^{2-}, and hence their OH vibrations may shift to lower wavenumbers than that of OH in Ca-OH. Thus, the strong peak at 3562 cm^{-1} in ettringite FTIR spectra is assigned to OH asymmetric stretching of Ca coordinated H_2O and the related symmetric stretching bands are at 3356 cm^{-1}. Corresponding Ca-OH vibrations are present at 3650–3600 cm^{-1} region.

ATR-FTIR spectra of aqueous SO_4^{2-} after background subtraction for bulk H_2O exhibit a broad band at the 3600–3100 cm^{-1} which resembles the broad OH band of H_2O in ettringite (Fig. 2). This suggests that H_2O in ettringite forms H-bonds with SO_4^{2-} in ettringite channels. In addition OH bending modes are also expected to display similar behavior, for example OH bending modes of H_2O in the solvation shell of SO_4^{2-}

vs. column H_2O in ettringite are 1655 and 1645 cm^{-1}, respectively. The ettringite OH bending vibrations are lower since H_2O also bonds with Ca and participates in H-bonding with SO_4^{2-}, which results in longer OH bond lengths.

3.1.2. SO_4^{2-} group vibrations

The SO_4^{2-} molecules in ettringite channels are hydrated completely and present in three crystallographically different sites in the unit cell (Fig. 1; Moore and Taylor, 1970). The S-O bond lengths at these three sites are: 1.51(1) and 1.56(3) Å; 1.36(1) and 1.49(3) Å; and 1.31(1) and 1.48(3) Å, where the number in parentheses indicates the total number of S-O bonds in a given SO_4^{2-} polyhedron of that bond length. All these polyhedra are different from aqueous SO_4^{2-} when compared for their S-O bond lengths (aq. SO_4^{2-}: 1.49 Å). This wide variation in S-O bond length for the uncomplexed SO_4^{2-} in ettringite (1.31–1.56 Å) may result from varying extents of H-bonding with structural H_2O (Moore and Taylor, 1970). From the bond lengths the symmetry of SO_4^{2-} polyhedra can be assigned to C_{3V}, but site-symmetry calculations made using ettringite crystal structure and local coordination of SO_4^{2-} suggests a C_1 symmetry (Fateley et al., 1971). A reduction in the symmetry of SO_4^{2-} from tetrahedral to either C_{3V} or C_1 (similar to AsO_4^{3-} described above) should split the triply (ν_3, ν_4) and doubly (ν_2, in the case of C_1 only) degenerate vibrations. The vibrational spectra of ettringite may provide this symmetry information, provided enough spectral resolution exists.

In dilute, neutral to alkaline pH solutions, SO_4^{2-} exhibits symmetric stretching and bending (ν_1, ν_2) and asymmetric stretching and bending (ν_3, ν_4) at approximately 983 (980), 450, 1105 (1098), and 611 cm^{-1}, respectively (Table 3; Nakamoto, 1986). The wavenumbers shown in parentheses are the bands for a dilute sodium sulfate aqueous solution (10 mM) collected with ATR-FTIR in the present study. Metal complexation, protonation, and/or hydration (in the case of hydrated solids) of one of the O in SO_4^{2-} results in an increase in that S-O bond length and consequently its S-OX (X = cation, H$^+$, or a H-bond) vibrations should shift to lower wavenumbers when compared to that of S-O$_{uncomplexed}$ vibrations of the same SO_4^{2-} polyhedra. Associated with these symmetry changes, the degeneracy on ν_2, ν_3, and ν_4 vibrations of this SO_4^{2-} group may also be lifted. Such spectral changes have been observed in the case of SO_4^{2-} adsorbed on mineral surfaces and inside crystalline solids (Table 3; Ross, 1974). Previous studies have indicated that the S-OX vibrations of SO_4^{2-} complexes (edge sharing and multidentate) in gypsum ($CaSO_4 \cdot 2H_2O$), anhydrite ($CaSO_4$), and bassanite ($CaSO_4 \cdot 0.5H_2O$) are at 1004, 1013, and 1012 cm^{-1}, respectively (Table 3; Ross, 1974). These vibrational frequencies are at higher wavenumbers as compared to the uncomplexed aqueous SO_4^{2-} ($\sim$ 983 cm^{-1}). Similarly, the average S-O bond lengths of SO_4^{2-} in all these compounds are also smaller than that of aqueous SO_4^{2-}. In contrast, complexes with high atomic number cations (e.g., Sr, Ba, Pb) exhibit S-OX vibrations at lower wavenumbers (965–980 cm^{-1}; Ross, 1974; Myneni, unpubl. data). Also the FTIR spectra of SO_4^{2-} adsorbed on Fe-oxyhydroxides indicated that the S-OFe vibrations are red-shifted when compared to that of aqueous SO_4^{2-} (Harrison and Berkheiser, 1982; Persson and Lovgren, 1996; Hug, 1997). In all these cases the S-O ν_3 and ν_4

Table 3. Normal modes of SO_4^{2-} in aqueous solutions and in crystalline solids relevant to ettringite. Sulfate complexes of Fe^{3+} are shown for comparison.

Species/Mineral	ν_1	ν_2	ν_3	ν_4
			(cm^{-1})	
SO_4^{2-}[a]	983	450	1105	611
Proton - SO_4^{2-} complexes (aqueous)				
SO_4^{2-}[b]	980$_{IR}$	--	1098$_{IR}$	
HSO_4^-[c]	891$_{IR(S-OH)}$	n.a	1051$_{IR(S-O)}$, 1194$_{IR(S-O)}$	n.a
Metal - SO_4^{2-} complexes (aqueous)				
$[Fe(III)SO_4]^{+}$[c]	980$_{IR(S-OFe)}$		1042$_{IR(S-O)}$, 1126$_{IR(S-O)}$	
$CaSO_4^0$[b]	978$_{IR(S-OCa)}$		1107$_{IR(S-O)}$ (broad)	
SO_4^{2-} complexes on mineral surfaces/ in crystals				
on α-FeOOH	980$_{IR(S-OFe)}$		1050$_{IR(S-O)}$, 1130$_{IR(S-O)}$,	
(goethite)[d]			1250$_{IR(S-O)}$	
on α-Fe$_2$O$_3$	976$_{IR(S-OFe)}$		1060$_{IR(S-O)}$, 1128$_{IR(S-O)}$	
(hematite)[e]				
Al$_2$(SO$_4$)$_3$·18H$_2$O	993, 960		1118, 1085	615
(alunogen)$_{IR}$[e]				
CaSO$_4$·2H$_2$O				
(gypsum) -IR[b]	1004	476	1102, 1119, 1146,	585, 604, 627,
Raman[f]	1016	417, 427,	1170	671
		495	1111, 1129, 1156	608, 628, 669,
				675
CaSO$_4$				
(anhydrite)-IR[e]	1013	515	1095, 1126, 1149	592, 612, 671
Raman[f]	1013	414, 495	1106, 1124, 1155	605, 624, 671
Ettringite$_{IR,R}$[b]	989 (br)	489, 451(sh)	1190, 1165, 1141,	669, 627, 606
			1098	

a: Nakamoto, 1986; b: This study; c: Hug, 1997; d: Persson and Lovgren, 1996; e: Ross, 1974; f: Hapanowicz and Condrate, 1996.

bands exhibit similar splitting (number of bands), and hence their spectral identification and interpretation are difficult. Nevertheless, the energy shifts of the S-OX symmetric and asymmetric stretches are noteworthy, and the relative shifts should correspond to the strengths of SO_4^{2-} interactions with complexing cations, protons, and/or solvated H$_2$O molecules. Also among the metal-sulfate complexes, the S-OM (M = metal) vibrations shift to higher wavenumbers with increasing metal coordination. For instance this band for the binuclear complexes is at a higher wavenumber than that of mononuclear complexes (Hezel and Ross, 1968). It should also be noted that, if certain metal atoms such as Ca do not distort the SO_4^{2-} polyhedron significantly, then the S-OM (M = metal) vibrations of binuclear complexes can be at higher wavenumbers than that of uncomplexed S-O symmetric stretching vibrations. In summary, these spectral features of metal complexes are very similar to the spectral behavior exhibited by the polyprotic arsenates and phosphates, which show shifts in the As-OH and P-OH bands to higher wavenumber with increases in proton concentration on the polyhedra (Cruickshank and Robinson, 1966; Myneni et al., 1998b). It can be concluded from existing data that the band positions of S-OX stretching vibrations for the protonated, metal complexed, and solvated species may be in the order H$^+$ ≪ metal ≤ H$_2$O (Table 3).

The FTIR and Raman spectra of SO_4^{2-} in ettringite exhibits vibrations around 1136, 989, 630, and 470 cm^{-1}, which correspond to the ν_3, ν_1, ν_4, and ν_2 vibrations, respectively (Fig. 2). All these bands have shoulders or overlapping peaks, and as mentioned earlier the ν_2 and ν_4 vibrations are difficult to distinguish in FTIR because of their overlap with the Ca/Al-OH bending modes. However, the Raman spectra of ettringite exhibit distinct bands corresponding to SO_4^{2-} ν_4 (669, 627, and 606 cm^{-1}) and ν_2 (489 and 451 cm^{-1}). These spectral features indicate that there is more than one type of structural SO_4^{2-} (from ν_1, discussed below), and its symmetry deviates from that of a symmetrical SO_4^{2-} tetrahedron (from split in ν_2, ν_3, ν_4 bands). These results support the previous X-ray crystal structure refinements of Moore and Taylor (1970). The center of mass for the ν_3 vibrations of SO_4^{2-} in ettringite shifted to higher wavenumbers (average ~ 1136 cm^{-1}) than that observed for aqueous SO_4^{2-} (1098 cm^{-1}). The former band is broad and consists of overlapping peaks at 1190, 1165, 1141, and 1098 cm^{-1} (Fig. 4), which likely correspond to the degenerate and nondegenerate modes of SO_4^{2-} occupying the three different crystallographic sites in ettringite (Moore and Taylor, 1970). Absence of distinctly split ν_3 vibrations, typically found in other calcium sulfate minerals, is noteworthy. In addition, the occurrence of one of the components of ν_3 at 1098 cm^{-1}, i.e., at the same wavenumber as that of aqueous SO_4^{2-}, may suggest that at least some of SO_4^{2-} polyhedra in ettringite may be very similar to that of aqueous SO_4^{2-}. Although the ν_3 band has a maxima at ~1131 cm^{-1} in Raman, the peak positions are not clearly separable since this band overlaps with the ν_1 band of CO_3^{2-} (Fig. 2).

The symmetric stretch of SO_4^{2-} occurs as a low intense band at ~989 cm^{-1} in FTIR and as strong peaks in Raman (Fig. 5). Since three symmetric stretching bands could be clearly identified from Raman spectral intensities, three components were used in fitting the broad FTIR band. A detailed examination of these SO_4^{2-} bands in both ettringite FTIR and Raman spectra shows three bands at 1016, 1008, and 989 cm^{-1} in Raman, and 1011, 996, and 982 cm^{-1} in FTIR, respectively (Fig. 5). These vibrations likely correspond to the crystallographically different SO_4^{2-} units in ettringite. Based on their relative energy positions, it can be hypothesized that the SO_4^{2-} polyhedra with S-O symmetric stretch at 1016 and 1008 cm^{-1} in Raman (or 1011, 996 cm^{-1}, respectively in FTIR) experiences weaker H-bonding inside the ettringite crystal than do SO_4^{2-} ions in aqueous solutions. X-ray crystal structure refinements indicate that two of the three SO_4^{2-} sites in the ettringite unit-cell have an average S-O bond length of 1.44 and 1.46 Å (or 1.48 & 1.49 Å as the longest bond lengths), i.e., smaller than that of aqueous SO_4^{2-} (Moore and Taylor, 1970). Hence, the SO_4^{2-} polyhedra responsible for the S-O ν_1 vibration above that of H$_2$O should reside in these two types of sites. Although binuclear complexation of SO_4^{2-} with Ca (as in calcium sulfates discussed above) can produce ν_1 band at a higher wavenumber (greater than that of tetrahedral SO_4^{2-} in water), absence of strong splitting in ν_3 band suggests that this may not be happening in ettringite. The third S-O symmetric stretch band (at 989 cm^{-1} in Raman and 982 cm^{-1} in FTIR) is more similar to that of aqueous SO_4^{2-}. However, Moore and Taylor (1970) reported that the third SO_4^{2-} group has a S-O bond length of ~1.55 Å. This is very close to the S-OH bond length in H$_2$SO$_4$ (1.54 Å; Moodenbagh et al., 1983) and slightly smaller than the S-OH bond
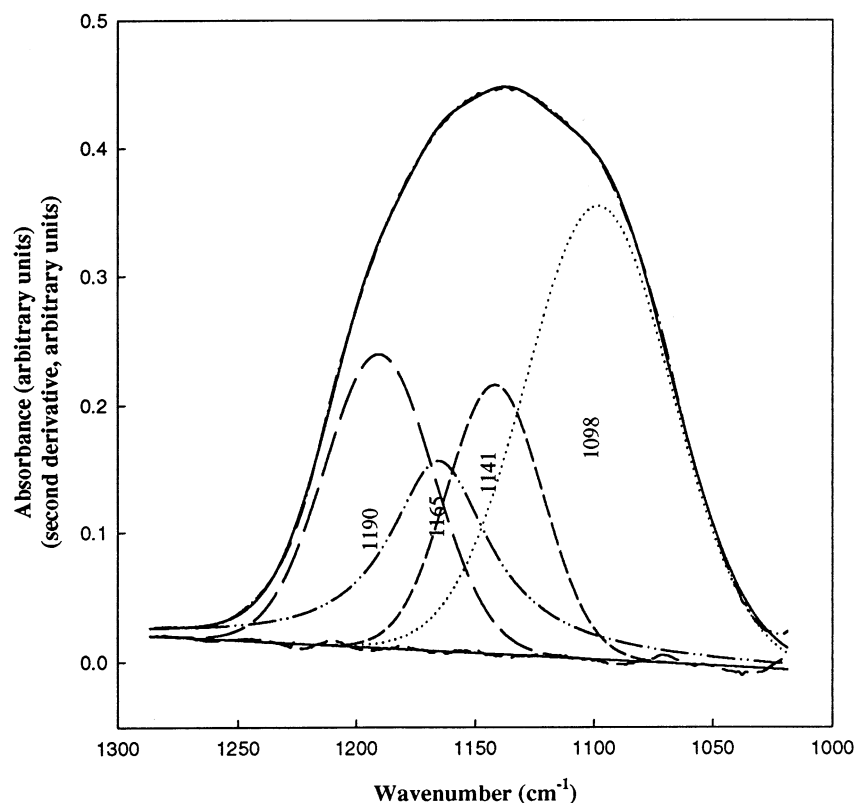
Fig. 4. Diffuse reflectance FTIR spectra of ettringite showing the S-O ν_3 vibrations. The spectra shown here contains the original spectrum, the deconvoluted peaks, fitted curve, residual, and the baseline.

length in HSO_4- (1.57 Å; Cruickshank and Robinson, 1966). These protonated sulfates exhibit S-OH symmetric stretch ≤ 920 cm^{-1} (Brown and Hope, 1995; Hug, 1997). Since the SO_4^{2-} polyhedra in ettringite only form H-bonds, bond lengths longer than those found in protonated SO_4^{2-} are unlikely. While vibrational spectra do not offer a measure of interatomic distances, they do provide a direct measure of the relative strength of bonding between SO_4^{2-} polyhedra and adjacent atoms. From the previous discussion, it seems likely that the exact structure of SO_4^{2-} polyhedra in ettringite is still unknown. It is of interest to note that Moore and Taylor (1970) also indicated some uncertainty in the assigned coordinates of S in the ettringite.

In summary, the vibrational spectra of SO_4^{2-} polyhedra in ettringite indicate two classes of SO_4^{2-} groups. Those with symmetric stretches close to that of aqueous SO_4^{2-} (i.e., ≤ 989 cm^{-1}) indicating the same type of H-bonding of SO_4^{2-} with structural H_2O in ettringite and the SO_4^{2-} polyhedra with symmetric stretches at higher wavenumbers than that of aqueous SO_4^{2-} form much weaker H-bonds with structural H_2O than those observed for SO_4^{2-} ions in aqueous solutions.

3.1.3. CO_3^{2-} Contamination in ettringite

Synthetic ettringite was prepared in CO_2-free deionized water, and thus this sample was expected to be free from CO_3^{2-} contamination. However, the occurrence of CO_3^{2-} ν_3 and ν_2 vibrations around 1450 cm^{-1} and 865 cm^{-1}, respectively, in ettringite FTIR spectra, and the ν_1 peak at 1080 cm^{-1} that overlaps the SO_4^{2-} asymmetric stretching band in the Raman

spectra indicate the presence of sorbed CO_3^{2-}. These bands have not been reported in previous IR studies of ettringite (Pöllmann et al.,1989; Kumarathasan et al., 1990). Despite the use of CO_2-free deionized water and N_2 (g) filled glove boxes in the ettringite synthesis, the spectra indicate that it is difficult to avoid CO_3^{2-} contamination in the final product. This CO_2 may have been introduced into ettringite through the reagents or from the atmosphere (during spectroscopic measurements).

3.2. AsO_4^{3-} Complexation in Ettringite

3.2.1. Arsenate solution chemistry and reactions with ettringite

While aqueous AsO_4^{3-} speciation usually has no direct bearing on what might exist at the mineral-water interfaces, knowledge on aqueous speciation can provide information on the nature of complexes that might occur in a given system. Aqueous solutions in contact with ettringite usually exhibit pH values in the range of 10.7–12.8 (Myneni et al., 1998a). The third pKa of arsenate is 11.49 (Dove and Rimstidt, 1985), and the dissolved arsenate can exist as AsO_4^{3-} and $HAsO_4^{2-}$ in the presence of ettringite. In addition, arsenate solutions in contact with ettringite may also have a fraction of the total soluble AsO_4^{3-} in the form of complexes with Ca^{2+} and Al^{3+}. To our knowledge, no thermodynamic constants are currently available to predict the concentration of these cation $-AsO_4^{3-}$ complexes at 298 K. However, recent studies on $CaAsO_4^-$ ion pairs in aqueous solutions at 313 K have indicated that the
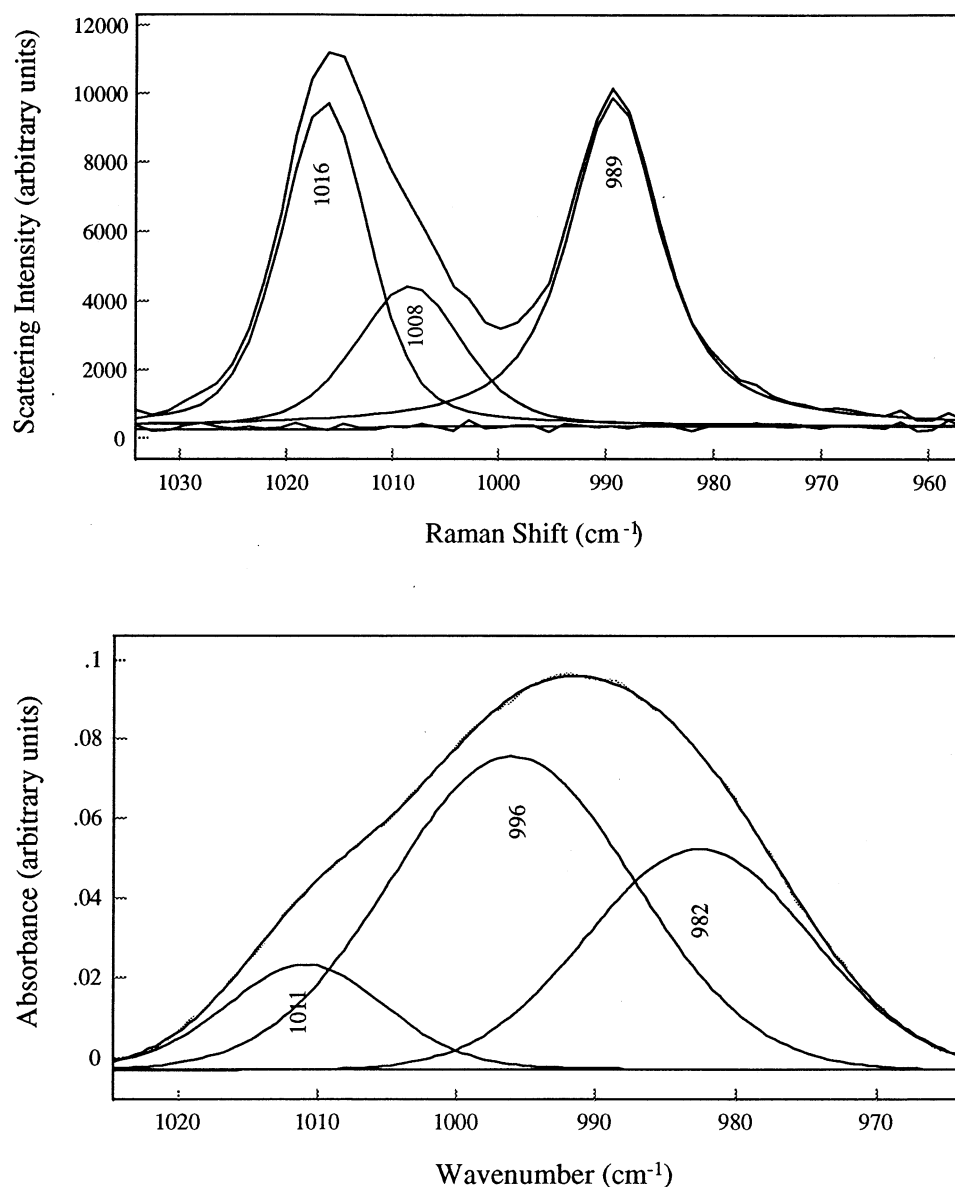
Fig. 5. Raman (top) and diffuse reflectance FTIR (bottom) spectra of S-O symmetric stretch in ettringite.

tendency for their formation is great in highly alkaline solutions (Mironov et al., 1995).

A summary of AsO_4^{3-} adsorption (reaction of synthetic ettringite with aqueous AsO_4^{3-}), and coprecipitation (precipitated ettringite from SO_4^{2-} and AsO_4^{3-} containing solutions) experiments is given in Table 4 (for a complete discussion, see Myneni et al., 1997). Coprecipitation resulted in more AsO_4^{3-} uptake than adsorption and in the former case the ettringite crystal structure was stable above the theoretical saturation limit of the reactive sites on the ettringite surface (0.11 mol kg^{-1}). However, when the solid phase AsO_4^{3-} concentration approached the point of surface saturation during adsorption experiments, poorly crystalline calcium arsenate solids and/or gypsum ($CaSO_4 \cdot 2H_2O$) precipitated at the expense of ettringite (Myneni et al., 1997). There was no correlation between the magnitude of AsO_4^{3-} sorption and solution pH suggesting that

aqueous AsO_4^{3-} speciation and ettringite surface charge did not play a critical role in AsO_4^{3-} sorption. From these results, Myneni and coworkers (1997) deduced that coprecipitation may result in AsO_4^{3-} channel substitution as well as sorption on exterior surfaces at low AsO_4^{3-} concentrations. Adsorbed AsO_4^{3-} only reacted with external surface sites. At high AsO_4^{3-} concentrations, surface interactions and precipitation of calcium arsenate(s) occurred during both adsorption and coprecipitation. If these proposed reactions do indeed occur, increases in the solid-phase concentration of AsO_4^{3-} and changes in the mode of sorption should produce changes in the peak intensities and positions of the vibrational bands of OH^-, H_2O, SO_4^{2-}, and AsO_4^{3-} in ettringite. As shown by X-ray crystal structure analysis of ettringite, the Ca and Al polyhedra are distorted strongly and their complexation with AsO_4^{3-} may not produce significant changes in their polyhedra. While Al-O

Table 4. Summary of AsO$_4^{3-}$ sorption in ettringite (for complete discussion, see Myneni et al., 1997).

Initial aqueous AsO$_4^{3-}$ concentration (mM)[†]	Sorption efficiency (%)	X-Ray diffraction	Scanning electron microscopy
AsO$_4^{3-}$ Adsorption			
0.017 (0.002)	> 99, No desorption	not different from that of ettringite	~ 2 μm ettringite grains
1.44 - 2.88 (0.14 - 0.27)	98 - 94	ettringite (100) reflections decreased, gypsum peaks present[#]	gypsum[#] + ettringite
5.76 (0.53)	92	ettringite completely disappeared[*]	gypsum with corroded surfaces[#]
15.2 (1.1)	73	ettringite and gypsum absent; presence of poorly crystalline material	fine grained, grain size < 1 μm
AsO$_4^{3-}$ Coprecipitation			
0.007- 0.216 (0.0035 - 0.108)	> 99	not different from that of ettringite	homogeneous size-distribution, long ettringite grains
AsO$_4^{3-}$ sorbed at high pH (~ 12.0), and in the presence of high SO$_4^{2-}$, is partly exchangeable.			
0.65 (0.33)	> 99	not different from that of ettringite	ettringite grain size decreased, heterogeneous grain size-distribution
1.44 (0.72)	> 99	ettringite + poorly crystalline material	heterogeneous grain sizes

[†] Numbers in parenthesis correspond to the solid phase AsO$_4^{3-}$ concentration in mol kg^{-1}.
[#] Gypsum was absent when adsorption was conducted by fixing the pH at 11.8.
[*] Ettringite was present when pH was maintained at 11.8, however, the base line of XRD patterns was not smooth.

vibrations could not be identified apparently in the ettringite vibrational spectra, the Ca-O vibrations at 327 and 360 cm^{-1} did not change with AsO$_4^{3-}$ sorption, indicating that at least the Ca polyhedra are little affected during the reactions (Fig. 6). Hence these vibrations will not be discussed further. Since AsO$_4^{3-}$ adsorption at high concentrations precipitated CaSO$_4 \cdot$ 2H$_2$O and calcium arsenate solids, these sample vibrational spectra not only indicate changes in the vibrational modes of ettringite, but also the spectral features corresponding to CaSO$_4 \cdot$ 2H$_2$O (H$_2$O bands at 3550, 3398, 1684, 1621 cm^{-1}; SO$_4^{2-}$ at 1147, 1118 cm^{-1}; Seidl et al., 1969; this research) and other AsO$_4^{3-}$ solids (not clearly separable).

3.2.2. Vibrational spectra of AsO$_4^{3-}$ in ettringite OH vibrations

The mode of AsO$_4^{3-}$ sorption (adsorption vs. coprecipitation), and aqueous AsO$_4^{3-}$ concentration and the solution pH perturbed the OH stretching frequencies (Fig. 7). With increases in solid phase AsO$_4^{3-}$ concentration, the OH peak maximum around 3562 cm^{-1} decreased (stronger in adsorption samples), and strong, broad OH bands around 3300 and 3000 cm^{-1} developed (adsorption and coprecipitation). In this latter case, this new band may have been due to the formation of H-bonds between AsO$_4^{3-}$ and structural OH or H$_2$O. Also the vibrational spectra of aqueous AsO$_4^{3-}$ (after subtracting for bulk water contributions) exhibits bands around 3350 and 3011 cm^{-1}, in agreement with these observations (Figs. 2 and 7). Similar H-bond formation between H$_2$O and AsO$_4^{3-}$ and appearance of a broad band around 3400–3000 cm^{-1} has also
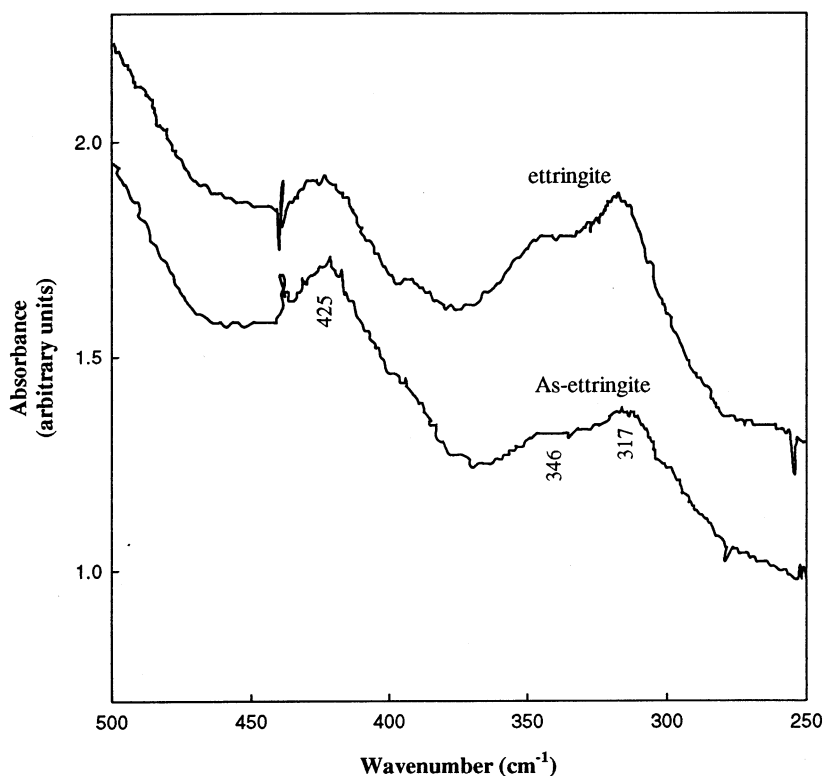

Fig. 6. The Far-IR spectra of ettringite showing the Ca-O vibrations in ettringite (top) and As-reacted ettringite (bottom).
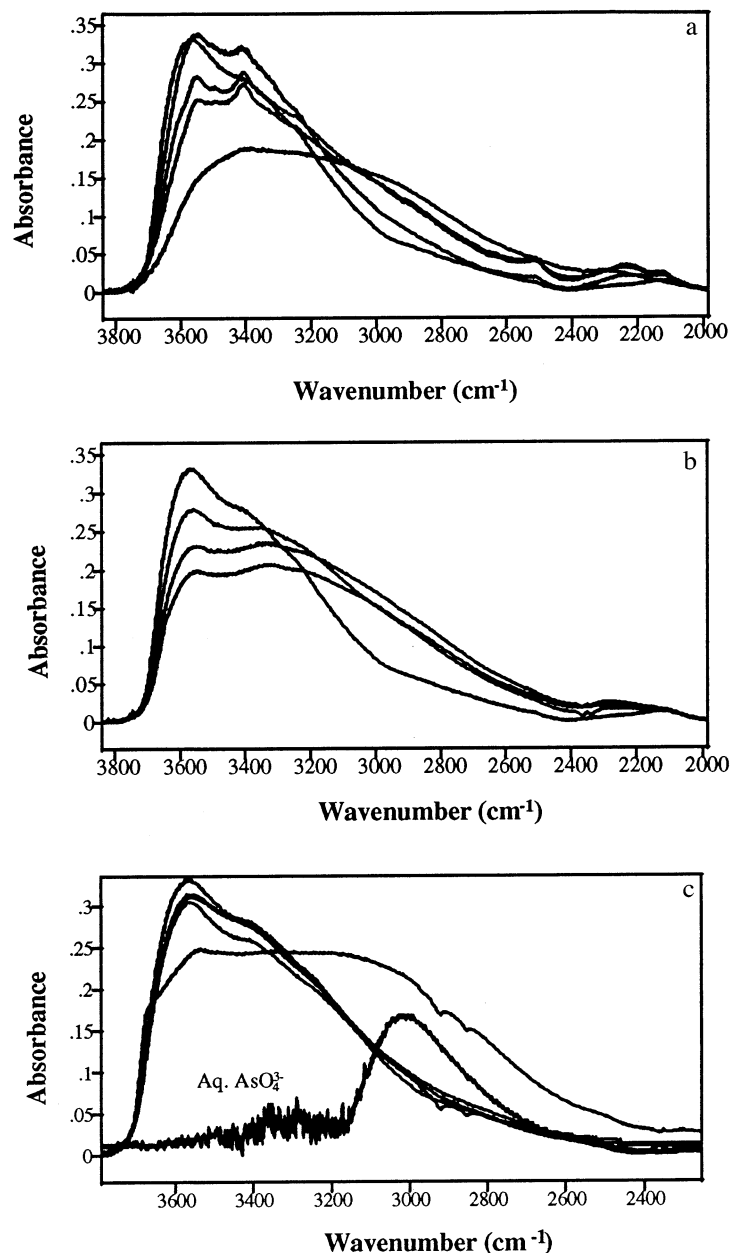
Fig. 7. The influence of AsO_4^{3-} sorption on ettringite OH vibrations. a and b are adsorption samples without and with pH control (11.8), respectively, and c shows the coprecipitation samples. In all, the spectrum with the maximum intensity around 3600 cm^{-1} is pure ettringite. The decreasing peak intensity at this wavenumber corresponds to increases in solid phase AsO_4^{3-} concentration. The OH vibrations of $HAsO_4^{2-}$ solvated H_2O is shown for comparison.

been reported from the arsenate solids of known crystal structure, such as $CaHAsO_4 \cdot 2H_2O$ and $Na_2HAsO_4 \cdot 7H_2O$ (Myneni et al., 1998b).

With increases in solid phase AsO_4^{3-} concentrations and irrespective of pH all adsorption samples showed decreases in peak intensity near 3562 and 3400 cm^{-1} (Fig. 7). Adsorption samples with solid phase AsO_4^{3-} concentrations of 6–20%, and no pH control, precipitated $CaSO_4 \cdot 2H_2O$ (Table 4; Myneni et al., 1997). Consequently the vibrational spectra of these samples exhibited sharp peaks related to OH and SO_4^{2-} vibrations (Figs. 7a, 8a). However, $CaSO_4 \cdot 2H_2O$ formation and corre-

sponding spectral changes were absent when the pH of the adsorption samples was maintained at 11.8 during sorption reactions (Fig. 7). In contrast, the coprecipitated samples did not exhibit significant changes in OH stretching frequencies at 3562 and 3400 cm^{-1}, irrespective of sample pH (10.5–12.5) and solid phase AsO_4^{3-} concentration (Fig. 7). However, a broad band around 3023 cm^{-1} and new sharp peaks at 3671, 3618, and 3542 cm^{-1} were produced with increases in solid phase AsO_4^{3-} concentration ($AsO_4^{3-} > 9\%$; Fig. 7).

The changes in the intensity of the broad peak around 3550 cm^{-1} peak likely correspond to the removal of Ca coordinated
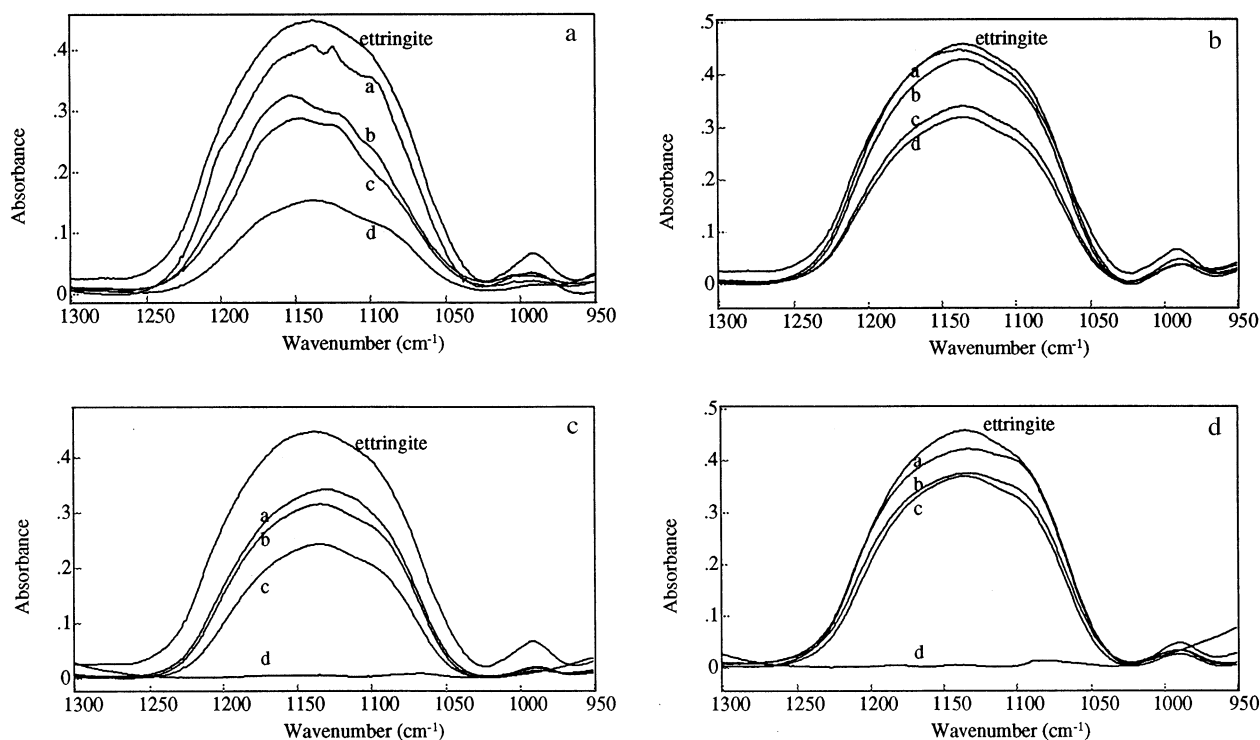
Fig. 8. Influence of AsO_4^{3-} sorption on ettringite S-O asymmetric stretching vibrations. a, b, c, and d correspond to the adsorption with no pH control, adsorption at pH 11.8, coprecipitation at 12.5, and coprecipitation at 12.0, respectively. Solid phase AsO_4^{3-} concentration increases in the order a < b < c < d. For coprecipitation samples, the sample d is prepared without any SO_4^{2-} in the system.

H_2O and/or Ca and Al coordinated OH at the ettringite surfaces. Since these changes are intense in adsorption samples, AsO_4^{3-} sorption may result in displacement of column OH or H_2O moieties. Absence of these stronger changes in the coprecipitated samples indicates that AsO_4^{3-} coprecipitation in ettringite did not occur predominantly through the displacement of structural OH or H_2O. Rather, it is likely that AsO_4^{3-} coprecipitation displaced SO_4^{2-} from ettringite channels, modifying H-bonding between the channel ions and intra-channel H_2O. In addition, development of new peaks at 3671, 3618, and 3542 cm^{-1} in concentrated coprecipitated samples may also indicate changes in OH moieties coordinated to Ca and/or Al and may relate to calcium arsenate precipitate identified in these sample XRD (Table 4; Myneni et al., 1997).

3.2.3 SO_4^{2-} vibrations

FTIR spectra of SO_4^{2-} in ettringite exhibited weak splitting in ν_3 band (maxima at 1136 cm^{-1}), with a broad ν_1 around 989 cm^{-1}. Recall, no splitting occurs for aqueous uncomplexed SO_4^{2-}. Only the low pH (<11.0), AsO_4^{3-} adsorption samples showed changes in the S-O ν_3 vibrations of SO_4^{2-}, causing splitting of the original band into two separate vibrations at 1156 and 1138 cm^{-1} (Fig. 8a, b). These were the samples in which $CaSO_4 \cdot 2H_2O$ precipitated at AsO_4^{3-} concentrations of 6–20%. Hence this band splitting has no relation to the symmetry of SO_4^{2-} in ettringite, but was caused by the precipitation of $CaSO_4 \cdot 2H_2O$ (see Table 3, Table 4). As indicated by the peak intensities, the structural SO_4^{2-} concentration of adsorp-

tion samples decreased with increases in the solid phase AsO_4^{3-} concentration. Although the coprecipitation samples exhibit the same trend, the samples prepared at low pH and high SO_4^{2-} did not show a major variation in structural SO_4^{2-} concentration (Fig. 8c,d).

With increases in solid phase AsO_4^{3-} concentration, the Raman spectra of the adsorption samples did not exhibit significant changes in the peak intensities of the ν_1 vibrations (Fig. 9). However, Raman spectra of the AsO_4^{3-} coprecipitated samples (irrespective of pH) showed an almost loss of S-O ν_1 components at 1016 and 1008 cm^{-1} with increases in solid phase AsO_4^{3-} concentration, while the S-O ν_1 band at 989 cm^{-1} showed little change. Since the peak intensities are related to SO_4^{2-} concentration in ettringite, decreases in S-O ν_1 bands at 1016 and 1008 cm^{-1} with increased AsO_4^{3-} coprecipitation into ettringite suggests preferential substitution of AsO_4^{3-} for SO_4^{2-} at these two of the three possible crystallographic sites within the channels. The broad, overlapping peaks in the FTIR spectra are less distinct, nevertheless spectral changes similar to those present in the Raman spectra were observed (Fig. 9).

3.2.4 AsO_4^{3-} vibrations

An overview of the theoretical and experimental vibrational spectra of AsO_4^{3-} has been presented in our earlier paper (Myneni et al., 1998b). These results indicate that the symmetry of AsO_4^{3-} is most greatly modified by protonation, and the relative influence of H^+-, cation-, and H_2O coordination on
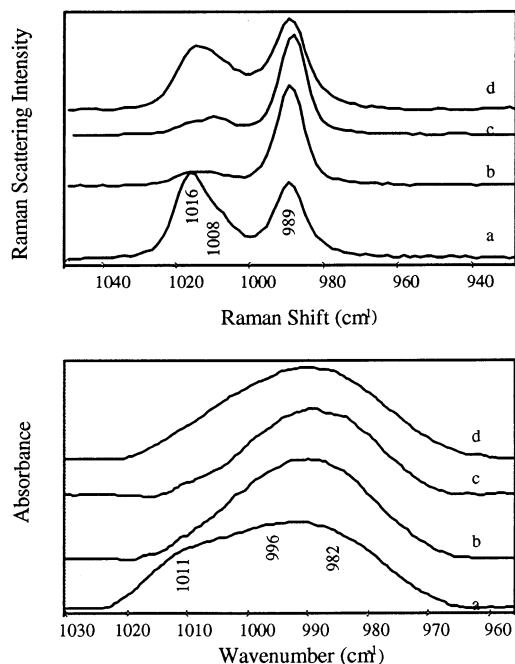
Fig. 9. Raman (top) and diffuse reflectance FTIR (bottom) spectra of S-O symmetric stretching vibrations in AsO_4^{3-} reacted ettringites. In both cases, (a) ettringite, (b and c) coprecipitated ettringite with 2 and 4% AsO_4^{3-}, respectively, and (d) adsorbed AsO_4^{3-} ettringite with 20% AsO_4^{3-}.

AsO_4^{3-}-symmetry decreases in the order $H^+ \gg$ cation $\leq H_2O$. As a result the As-OX (X = H^+, cation, H_2O) stretching frequencies of these complexes shift to different wavenumbers. In the case of polyprotic arsenate complexes, the As-OH symmetric stretch shifted to higher wavenumbers ($H_3AsO_4^0 > H_2AsO_4^- > HAsO_4^{2-}$) with increasing proton number of the complex. It should be noted that the symmetric As-OH in $H_3AsO_4^0$ is usually at a lower wavenumber than the As-O symmetric stretching in AsO_4^{3-} (Myneni et al., 1998b). Similarly, metal complexation in the form of monodentate and bidentate binuclar complexes are also expected to exhibit the same behavior (As-OM bond length for these complexes may increase in the order M-AsO_4^{3-} > M_2-AsO_4^{3-}; however, this behavior is only seen for unprotonated metal-arsenate complexes. This is because the proton greatly distorts the AsO_4^{3-} polyhedron and typically controls its group frequencies, and metal complexation of protonated AsO_4^{3-} does not modify AsO_4^{3-} group frequencies further. This was observed in several calcium arsenate solids of known crystal structure (Myneni et al., 1998b)). Since metal complexation does not shift the As-OM (where M = metal) stretching vibrations to very low wavenumbers (unlike protonated AsO_4^{3-}), very often the polynuclear complexes (e.g., bidentate binuclear) can exhibit As-OM stretching vibrations at a higher wavenumber than the As-O symmetric stretching of the uncomplexed AsO_4^{3-} (recall the discussion for sulfato complexes).

Arsenate sorption in ettringite may occur through the sorption of protonated and/or unprotonated arsenate and complexes with ettringite functional groups in different symmetries (e.g., monodentate, bidentate). The experimental data on As-O vibrations indicate that they are different in adsorption and co-precipitation samples (Fig. 10, Table 5). The FTIR and Raman of these samples exhibited weak splitting in the As-O ν_3 vibrations, which overlapped each other, As-O ν_1 band, and CO_3^{2-} and Al-OH bending vibrations.

3.2.5 Adsorption samples

Peak deconvolution of spectra from adsorption samples showed weak splitting for As-O ν_3 vibrations (947, 900, 842 cm^{-1}), independent of sample pH, and increases in AsO_4^{3-} concentrations for samples with solid-phase AsO_4^{3-} concentrations $\geq$ 25 mmol kg^{-1} (Fig. 10). At these concentrations, ettringite surface sites are close to the saturation (maximum site density 0.11 mol kg^{-1}; Myneni et al., 1997). Consequently, the samples examined with FTIR and Raman correspond to the transition from surface reactions to precipitation of calcium arsenate. Although splitting of the ν_3 vibrations indicated a decrease in symmetry of the AsO_4^{3-}, it provided little information about its bonding environment. This ν_3 splitting is indicative of either C_{2v} or C_1 AsO_4^{3-} symmetry, as well as a mixture of high and low symmetry species.

The As-OX (X = Ca, Al, H_2O, and/or H^+) stretching vibrations showed distinct changes. In the absence of pH control, As-OX stretching modes produced two bands at 807 and 787 cm^{-1} in ettringite samples with AsO_4^{3-} $\leq$ 2%. From the presence and position of these bands at these wavenumbers, it can be hypothesized that the AsO_4^{3-} ion is bound predominantly to Ca atoms in bidentate binuclear (807 cm^{-1}) and monodentate mononuclear complexes (787 cm^{-1}). Alternately these band positions may also indicate the asymmetric and symmetric stretching vibrations of the same As-OCa complex (symmetry lower than C_{2v}), but their relatively high intensities in IR spectra makes this unlikely. The predicted complexes should produce both As-OCa symmetric and asymmetric stretching, but due to the strong overlap of these bands, only their average behavior was identified.

With increases in AsO_4^{3-} concentration (>2%), the As-OCa band at 807 cm^{-1} remained stable indicating the persistence of bidentate binuclear complexes, while the other decreased in intensity. New peaks which can be assigned to the As-OH stretching vibrations developed at 748 cm^{-1}, respectively, and were very distinct in samples with pH < 11.2 (Fig. 10a). During the sorption reaction, the solution pH in these samples dropped from 11.4 (solid phase AsO_4^{3-} = 2%) to 10.9 (solid phase AsO_4^{3-} = 20%; Myneni et al., 1997). In this pH range, the ratio of aqueous concentrations of $HAsO_4^{2-}/AsO_4^{3-}$ increases with decreasing pH (pKa = 11.49). Thus, the FTIR bands around 748 cm^{-1} may be due to the direct sorption of $HAsO_4^{2-}$ into ettringite or precipitation of a calcium monohydrogen arsenate. As expected, this band was not observed in adsorption samples when a pH of 11.8 was maintained throughout the reaction, indicating adsorption or precipitation of unprotonated AsO_4^{3-} species (Fig. 10b). It should be noted that the symmetry of protonated arsenate complexes are difficult to predict; and the As-O vibrations of the concentrated samples correspond to both the AsO_4^{3-} species in ettringite and also from those of Ca/Al arsenate precipitates (discussed earlier, Table 4).

Arsenate complexation with $\equiv$Al-OH sites of ettringite can
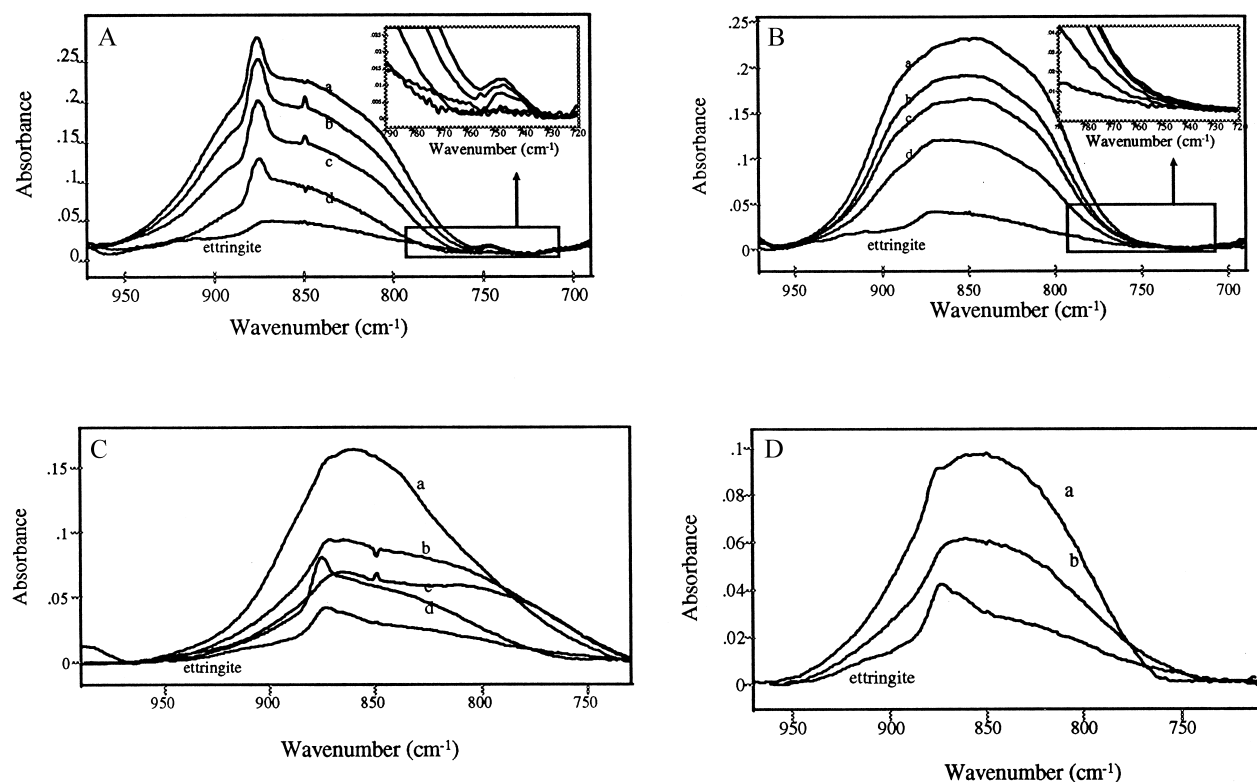
Fig. 10. As-O stretching vibrations of AsO_4^{3-} adsorbed (A, B) and coprecipitated ettringite (C, D). The solid phase AsO_4^{3-} concentrations of adsorption samples (in %) are, (a) 20, (b) 17, (c) 6, and (d) 2. The adsorption samples shown in (A) are prepared in the absence of pH control, and those in B are prepared at pH 11.8. The solid phase AsO_4^{3-} concentrations (in %) in C (pH = 12.5) are (a) 20, (b) 9, (c) 4 (with more Al^{3+}), and (d) 4; and in D (pH = 12.0) are (a) 20 and (b) 4.

not be determined unambiguously from the vibrational spectra. The vibrational spectra of a poorly crystalline aluminum arsenate has been shown to exhibit As-OAl stretching vibrations at 740 cm^{-1} (Myneni et al., 1998b). Although these authors have not ruled out the presence of protonated arsenate in this poorly crystalline Al-arsenate, the high intensity of this band at 740 cm^{-1}, together with the presence of a broad band at 887 cm^{-1} corresponding to As-O$_{uncomplexed}$, may indicate that these vibrational bands may have been caused by Al complexation with arsenate. For this reason the occurrence of an As-OM (M = metal) band above 780 cm^{-1} for As-ettringite may indicate that AsO_4^{3-} complexes predominantly with Ca rather than Al sites. However, appearance of peaks around 750 cm^{-1} in some low pH adsorption samples does not rule out the presence of Al-arsenate complexes in this system, but these may occur at very low concentrations. This is because arsenate sorption at these low pH values (~10.7) and at high arsenate concentrations, Al was ejected out of ettringite crystal structure and was present dominantly in the aqueous phase (Myneni et al., 1997). More experimental studies on aluminum arsenate are required to support these theoretical studies and the proposed hypothesis.

3.2.6 Coprecipitation samples

The coprecipitated AsO_4^{3-} ettringite samples showed complex FTIR patterns (Fig. 10c,d). Coprecipitation experiments were conducted at pH 12.5 and 11.8 and the latter samples with relatively high SO_4^{2-} concentration. Although pH has no effect on AsO_4^{3-} sorption (Myneni et al., 1997), the FTIR spectra of these samples indicate that high SO_4^{2-} concentrations in the solid had a major influence on AsO_4^{3-} symmetry. The coprecipitated samples with AsO_4^{3-} concentrations $\leq 4\%$ exhibit very little splitting in As-O ν_3 vibrations (Table 5). Also concentrated AsO_4^{3-} samples produced at pH = 12.5 showed more As-O stretching vibrational bands than those prepared at pH 12.0 (Fig. 10d). Apparently, the higher pH samples contained AsO_4^{3-} in several different local coordinations, and in lower symmetries than the lower pH, high SO_4^{2-} samples. The As-OX stretching vibrations exhibit peaks around 800 and 760 cm^{-1} that overlap with As-O$_{uncomplexed}$ vibrations. These band positions indicate that AsO_4^{3-} again interacts dominantly with Ca in the form of binuclear and mononuclear complexes, rather than with Al.

3.3. Summary of AsO_4^{3-} coordination in ettringite

In summary, ettringite FTIR and Raman spectroscopic studies have offered valuable information on the chemistry of ettringite reactive functional groups, and for the most part this data is in agreement with the previous X-ray crystal structure refinement studies. The vibrational spectroscopy studies have indicated that the reactive OH and H$_2$O sites linked to Ca/Al atoms cannot be distinguished unambiguously because of the

Table 5. Normal modes of AsO₄²⁻ in aqueous solutions and in ettringite.

Aqueous Species	Symmetric Stretching[†]	Asymmetric Stretching[†]
	(± 5 cm⁻¹)	
AsO_4^{3-} [a]	814	794
$HAsO_4^{2-}$ IR[b]	680-700(As-OH), 846(As-O)	865(As-O)
$H_2AsO_4^-$ IR[b]	759-766(sym. & as. As-OH), 875(As-O)	908(As-O)
$H_3AsO_4^0$ R[c]	769(As-OH), 973(As-O)	808(As-OH)

Solid Phase As Concentration (%)	As-OCa	As-O uncomplexed
	(± 15 cm⁻¹)	
Adsorption		
2 (pH 11.4)	808, 787	947, 900, 842
4 - 20 (pH 11.2 - 10.9)	808, 787, 748 As-OH	947, 900, 842
Coprecipitation		
1.4 (pH 11.8)		861 (sh), 847 (s)
4 - 20 (pH 12. 4)	801 (s), 776	989, 910, 880 (s), 863
4 (pH 11.8)	795 (s), 758 (sh)	915 (br), 830 (s)
9 - 20 (pH 11.8)	758 (w)	937, 915, 885 (s), 835
30* (pH 12. 5)	793, 769	957, 935, 883 (s), 852

Superscripts: a: Eysel and Wagner, 1993; b: Myneni et al., 1998b; c: Vasant et al., 1973.
Subscripts: IR: infrared, R: Raman
Symbols in brackets: s: strong, sh: shoulder, w: weak, br: broad
* SO_4^{2-}/AsO_4^{3-} ratio in the reacting solutions was zero.
† In the case of AsO₄³⁻ complexation in ettringite, strong overlapping of the bands prevents accurate identification of As-O symmetric and asymmetric stretching vibrations. For this reason, the As-O complexed, and As-O uncomplexed are given separately.

strong overlap in the OH stretching region. The SO_4^{2-} polyhedra of the three crystallographically different sites in ettringite occur in two different chemical environments. Two of the three SO_4^{2-} polyhedra exhibit weaker H-bonding with structural water and have the S-O symmetric stretch at a higher wavenumber than that of aqueous solutions. In contrast, the SO_4^{2-} polyhedra at the third site has the H-bonding environment very similar to that of aqueous solutions, and this contradicts the S-O bond lengths of this SO_4^{2-} polyhedra reported by Moore and Taylor (1970).

Arsenate sorption in ettringite caused significant changes in ettringite OH/H_2O and SO_4^{2-} vibrations, which varied as a function of solid phase AsO_4^{3-} concentration, mode of sorption, and pH. The vibrational spectra of adsorption samples exhibited features that are indicative of displacement of structural OH/H_2O units with increases in sorbed AsO_4^{3-} concentration. This suggests that AsO_4^{3-} forms inner-sphere complexes in all adsorption samples, either as monodentate-mononuclear/binuclear and/or bidentate-mononuclear/binuclear complexes by displacing surface hydroxyls. Based on the location of As-OCa bands around 800 cm⁻¹ the probable complexes are tentatively identified as monodentate-mononuclear and bidentate-binuclear. With increases in solid phase AsO_4^{3-} concentration, the bidentate-binuclear complexes remained stable and the relative concentration of monodentate-mononuclear complexes decreased. Channel substitution was insignificant during adsorption because AsO_4^{3-} adsorption had no influence on channel SO_4^{2-} and its concentration. Although sample pH did not affect local coordination of sorbed AsO_4^{3-} in ettringite, $HAsO_4^{2-}$ was also one of the adsorbed species at solution pHs < 11.2.

Although Al-arsenate complexes can form in these samples prepared at pH < 11.2, their presence have to be validated with other complimentary spectroscopic methods (Myneni et al., 1998b).

The coprecipitated samples exhibit similar AsO_4^{3-} bonding environments as adsorption samples at high sorption densities. However, little disturbance to the structural OH/H_2O moieties and complete displacement of weakly H-bonded SO_4^{2-} from channel sites indicate that AsO_4^{3-} preferentially substituted for SO_4^{2-} inside the channels at low sorption densities. This does not rule out the presence of surface complexes, but their concentration must be small relative to the occupation of channel sites. Little perturbation in As-O vibrations of dilute AsO_4^{3-} samples may suggest that AsO_4^{3-} forms outer-sphere complexes inside the channels of ettringite, in agreement with the previous bond valence estimates (Myneni et al., 1997).

In conclusion, these studies have provided incite on the functional group chemistry of ettringite and the location of sorbed AsO_4^{3-} in the ettringite structure. The desorption of sorbed AsO_4^{3-} and the energetics (free energy change and reaction rates) of its redox transformations is primarily determined by the location of the sorbed AsO_4^{3-} in ettringite structure and its coordination chemistry. Since AsO_4^{3-} coprecipitation results in ettringite channel substitution, such reactions are more favorable for reducing AsO_4^{3-} solubility in the environment. Under these conditions the sorbed AsO_4^{3-} may not be available for further chemical transformations unless ettringite crystals undergo dissolution. Vibrational spectroscopy of ettringite containing alkaline materials can provide clues to the structural location of AsO_4^{3-} and other oxoanions. This information is critical in predicting the geochemistry of alkaline ettringite containing materials and in selecting the appropriate remediation strategies for the treatment of contaminated sites.

REFERENCES

Barger J. R., Towle S. N., Brown Jr., G. E., and Parks G. A. (1997) XAFS and bondvalence determination of the structures and compositions of the surface functional groups and Pb(II) and Co(II) sorption products on single-crystal (α-Al₂O₃. *J. Colloid Interface Sci.* **185,** 473–492.

Bishop J. L., Pieters C. M., and Edwards J. O. (1994) Infrared spectroscopic analysis on the nature of water in montmorillonite. *Clays Clay Minerals* **42,** 702–716.

Brown G. M. and Hope G. A. (1995) In situ spectroscopic evidence for the adsorption of SO_4^{2-} ions at a copper electrode in sulfuric acid solution. *J. Electroanal. Chem.* **382,** 179–182.

Brown I. D. and Altermatt D. (1985) Bond-valence parameters obtained from a systematic analysis of the inorganic crystal structure database. *Acta Cryst.* **B 41,** 244–247.

Cruickshank D. W. J. and Robinson E. A. (1966) Bonding in orthophosphates and orthosulfates. *Spectrochim. Acta* **22,** 555–563.

Dove P. and Rimstidt D. (1985) The solubility and stability of scorodite. *Amer. Mineral.* **70,** 838–844.

Eysel H. H. and Wagner R. (1993). Raman intensities of liquids: Absolute scattering activities and electro-optical parameters (EOPs) of arsenate and selenate ions in aqueous solutions. *Spectrochim. Acta.* **49 A,** 503–507.

Fadini A. and Schnepel F.-M. (1989) *Vibrational Spectroscopy.* Ellis Horwood Ltd.

Farmer V.C. (1974) *The infrared Spectra of Minerals.* Miner. Soc.

Fateley W. G., Mcdevitt N. T., and Bentley F. F. (1971) Infrared and Raman selection rules for lattice vibrations: The Correlation Method. *Appl. Spectr.* **25,** 155–173.

Fowler R. K., Traina S. J., Bigham J. M., and Soto U. I., 1993. Solution chemistry and mineralogy of Clean Coal Technology By-products in a long term equilibration study. *Ag. Abst.*, 30.

Hapanowicz R. P. and Condrate R. A., Sr. (1996) Raman spectral investigation of sulfate inclusions in sodium calcium silicate glasses. *J. Solid State Chem.* **123,** 183–185.

Harrison J. B. and Berkheiser V. (1982) Anion interactions with freshly prepared hydrous iron oxides. *Clays Clay Minerals* **30,** 97–102.

Hayes K. F., Roe A. L., Brown G. E. Jr., Hodgson K. O., Leckie J. O., and Parks G.A. (1987) In situ X-ray absorption study of surface complexes: selenium oxyanions on (−FeOOH. *Science* **238,** 783–786.

Hezel A. and Ross S. D. (1968) Forbidden transitions in the infra-red spectra of tetrahedral anions-IV. The vibrational spectra (4000-400 cm-1) of some cobalt (III) sulphato- and phosphato-complexes. *Spectrochim. Acta* **24A,** 985–992.

Hingston F. J., Atkinson R. J., Posner A. M., and Quirk J. P. (1967) Specific adsorption of anions. *Nature* **215,** 1459–146.

Hug S. (1997). In situ Fourier Transform infrared measurements of sulfate adsorption on hematite in aqueous solutions. *J. Colloid Inerface Sci.* **188,** 415–422.

Kumarathasan P., Mccarthy G. J., Hassett D. J. and Hassett D. F. P. (1990) Oxyanion substituted ettringites: Synthesis and characterization and their potential role in immobilization of arsenic, boron, chromium, selenium, and vanadium. In *Fly Ash and Coal Conversion By-Products: Characterization, Utilization and Disposal* (ed. R. L. Day and F. P. Glasser); *VI. Mat. Res. Symp. Proc.* **178,** 83–103.

Linklater C. M., Albinsson Y., Alexander W. R., Casas I., Mckinley I. G., and Sellin P. (1996) A natural analogue of high pH cement pore waters from Maqain area of Northern Jordan: Comparison of predicted and observed trace element chemistry of uranium and selenium. *J. Cont. Hydrol.* **21,** 59–69.

Maddoms W. F. (1980) The scope and limitations of curve fitting. *Appl. Spectr.* **34,** 245–267.

Mattigod S. V., Rai D., Eary L. E., and Ainsworth C. C. (1990) Geochemical factors controlling the mobilization of inorganic constituents from fossil fuel combustion residues: I. Review of the major elements. *J. Environ. Qual.* **19,** 187–201

Mehta P. K. and Monteiro P. J. M. (1993) *Concrete: Structure, Properties, and Materials.* 2nd ed. Prentice Hall.

Mironov V. E., Kiselev V. P., Egizaryan M. B., Golovnev N. N., and Pashkov G. L. (1995) Ion association in aqueous solutions of calcium arsenate. *Rus. J. Inorg. Chem.* **40,** 1690–1691.

Moenke H. (1962) *Mineralspektren* I. Akademie-Verlag.

Moodenbaugh A. R., Hartt J. B., and Hurst J.. (1983) Neutron Diffraction study of polycrystalline H2SO4 and H2SeO4. *Phys. Rev.* **B 28,** 3501–3505.

Moore A. E. and Taylor H. F. W. (1970) Crystal structure of ettringite, *Acta Cryst.* **B26,** 386.

Mulcahy F. M., Fay M. J., Proctor A., Houalla M., Hercules D. M. (1990) The adsorption of metal oxoanions on alumina. *J. Calal.* **124,** 231–240.

Myneni S. C. B. (1995) Oxyanion-Mineral Surface Interactions in Alkaline Environments: Arsenate and Chromate Sorption and Desorption in Ettringite. Ph. D Dissertation. 252 p.

Myneni S. C. B. Traina S. J., Logan T. J., and Waychunas G. A. (1997) Oxyanion behavior in alkaline environments: Sorption and desorption of arsenate in ettringite. *Environ. Sci. Tech.* **31,** 1761–1768.

Myneni S. C. B., Traina S. J., and Logan T. J. (1998a) Ettringite Solubility and Geochemistry of the Ca(OH)₂-Al₂(SO₄)₃-H₂O System at 1 atm Pressure and 298 K. *Chem. Geol.* **148,** 1–19.

Myneni S. C. B., Traina S. J., Waychunas G. A., and Logan T. J. (1998b) Experimental and theoretical vibrational spectroscopic evaluation of arsenate coordination in aqueous solutions, solids, and at mineral-water interfaces. *Geochim. Cosmochim. Acta* **62,** 3285–3300.

Nakamoto K. (1986) *Infrared and Raman Spectra of Inorganic and Coordination Compounds.* Wiley.

Parfitt R. L., Russell J. D., and Farmer V. C. (1976) Conformation of the surface structures of goethite (α-FeOOH) and phosphated goethite by infrared spectroscopy. *J. Chem. Soc. Faraday I.* **72,** 1082–1087.

Persson P., Nilsson N., and Sjöberg S. (1996). Structure and bonding of orthophosphate ions at the iron oxide-aqueous interface. *J. Colloid Intl. Sci.* **177,** 263–275.

Persson P., and Lövgren L. (1996) Potential and spectroscopic studies of sulfate complexation at the goethite-water interface. *Geochim. Cosmochim. Acta* **60,** 2789–2799.

Pöllmann H., Kuzel H.-J., and Wenda R. (1989) Compounds with ettringite structure. *N. Jb. Miner. Abh.* **160,** 133–158.

Reeder R. J., Lamble G. M., Lee J., and Staudt W. J. (1994) Mechanism of SeO₄²⁻ adsorption in calcite: An EXAFS study. *Geochim. Cosmochim. Acta* **58,** 5639–5646.

Ross S. D. (1974) Phosphates and other oxy-anions of group V. In *The Infrared Spectra of Minerals* (ed. V. C. Farmer), pp. 383–422. Mineral. Soc. London.

Siedl V. and Knop O. (1969) Infrared studies of water in crystalline hydrates: Gypsum, CaSO₄.2H₂O. *Canadian J. Chem.* **47,** 1362–1368.

Tejedor-Tejedor I. M. and Anderson M. (1986). In situ Attenuated total reflection Fourier Transform infrared studies of the goethite (α-FeOOH)-aqueous solution interface. *Langmuir* **2,** 203–210.

Vasant F. K., Van Der Veken B. J., and Desseyn H. O. (1973) Vibrational analysis of arsenic acid and its anions. I Description of the Raman spectra. *J. Mol. Structure* **15,** 425–437.

Waychunas G. A., Rea B. A., Fuller C. C., and Davis J. A. (1993) Surface chemistry of ferrihydrite: Part 1. EXAFS studies of the geometry of coprecipitated and adsorbed arsenate. *Geochim. Cosmochim. Acta* **57,** 2251–2269.